

Flagellar number governs bacterial spreading and transport efficiency

Javad Najafi,^{1,*} M. Reza Shaebani,^{2,*} Thomas John,¹ Florian Altegoer,³ Gert Bange,³ and Christian Wagner^{1,4,†}

¹*Department of Experimental Physics, Saarland University, 66123 Saarbrücken, Germany.*

²*Department of Theoretical Physics, Saarland University, 66123 Saarbrücken, Germany.*

³*Department of Chemistry and LOEWE Center for Synthetic Microbiology,*

Philipps University Marburg, 35043 Marburg, Germany.

⁴*Physics and Materials Science Research Unit, University of Luxembourg, 1511 Luxembourg, Luxembourg.*

Peritrichous bacteria synchronize and bundle their flagella to actively swim while disruption of the bundle leads to tumbling. It is still not known whether the number of flagella represents an evolutionary adaptation towards optimizing bacterial navigation. Here, we study the swimming dynamics of differentially flagellated *Bacillus subtilis* strains in a quasi-two-dimensional system. We find that decreasing the number of flagella N reduces the average turning angle between two successive run phases and enhances the duration and directional persistence of the run phase. As a result, having less flagella is beneficial for long-distance transport and fast spreading, while having a lot of flagella is advantageous for the processes which require localization and slow dynamics, such as biofilm formation. We develop a two-state random walk model that incorporates spontaneous switchings between the states and yields exact analytical expressions for transport properties, in remarkable agreement with experiments. The results of numerical simulations based on our two-state model suggest that the efficiency of searching and exploring the environment is optimized at intermediate values of N . The optimal choice of N , for which the search time is minimized, decreases with increasing the size of the environment in which the bacteria swim.

INTRODUCTION

Many bacterial species swim by the rotation of flagella [1]. Several flagellation patterns can be distinguished according to the flagellar arrangement on the cell body, ranging from polar (one flagellum at one pole) to peritrichous (helical arrangement on the whole cell body) [2]. Each flagellum is anchored within the cell membrane to a reversible rotary motor that switches between clockwise and counter-clockwise rotation [3]. The ability of the motor to turn in either direction allows *polarly-flagellated* bacteria, such as *Caulobacter crescentus*, to change the swimming direction of the cell [4]. A *peritrichously-flagellated* bacterium experiences an alternating sequence of active runs and tumbles [5], controlled by the rotational states of each flagellum. When all flagella rotate counter-clockwise, they form a bundle and synchronize their rotation. As a result, the bacterium moves forward smoothly (run phase). However, the bundle is disrupted when some of the flagella switch their rotational direction, which facilitates changes in the direction of motion in relatively short time intervals (tumble phase). The *run-and-tumble* dynamics of bacteria allows them to change their direction of motion. They can also adjust the duration of stay in the run phase in response to environmental changes induced, e.g., by temperature, light, or chemical gradients [1, 5]. Such an ability is known to be highly advantageous to enhance search efficiency [6–8], allowing for an optimal navigation towards favorable or away from harmful regions [9].

Despite the advances in understanding of the underlying mechanisms of bundle formation and disruption [10–17] and its relationship to the chemotaxis signaling network [1, 9, 18, 19], it remains poorly understood how the number of flagella influences the fundamental properties of bacterial propulsion and transport. Attempts to understand the role of flagellation have mainly focused on *Escherichia coli* which has up to eight flagella, while the flagellar number of many types of bacteria is typically much higher. So far, it has been observed that the torque and thus the swimming speed [11] and the fraction of time spent in run or tumble phase [12] of peritrichously-flagellated bacteria remain roughly independent of the flagellar number N_f . Recent numerical studies also predict that the swimming speed is only slightly affected by N_f , assuming that just a single bundle is formed [20, 21]. Here, we provide evidences for the formation of multiple bundles, revealing that the former assumption does not hold at least at high flagellar number.

A key question from an evolutionary point of view is based on which criteria a bacterium chooses to have a certain number of flagella. In the present study, we investigate bacterial motility over a wide range of the flagellar number and clarify how the run-and-tumble dynamics is influenced by the choice of N_f . We study *Bacillus subtilis*, a rod-shaped bacterium commonly found, e.g., in soil and the gastrointestinal tract of humans. The number of flagella is regulated by the master regulator *swrA* in *Bacillus subtilis* [22]. Deletion of the gene leads to a reduction from 26 to 10 flagella, while cells overexpressing *swrA* exhibit up to 40 flagella. Therefore, we employed a wild-type *Bacillus subtilis* (NCIB3610 strain) with 26 flagella, a $\Delta swrA$ strain

* J. N. and M. R. S. contributed equally to this work.

† Corresponding author. Email: c.wagner@mx.uni-saarland.de

deficient for *swrA* (9 flagella), and a one which carries *swrA* under the control of an IPTG-inducible promoter (41 flagella) (Fig.1A). While the speeds in both run and tumble phases and the mean duration of tumbling periods show no systematic dependence on N_f , the duration and directional persistence of the run phase and the average turning angle between two successive run phases vary monotonically with N_f . Smaller values of N_f are more favorable for long-distance transport and fast spreading because of more persistent trajectories and longer excursion times in the run phase. On the other hand, increasing N_f facilitates tumbling, leading to slow dynamics and localization which is beneficial e.g. for the formation of biofilms. We develop a coarse-grained analytical approach to study the run-and-tumble dynamics of bacteria, which enables us to identify the contributions of the influential factors and map out the phase diagrams in the space of the relevant parameters of run-and-tumble statistics. Our simulation results suggest that by adopting intermediate values of N_f (as e.g. in the wild-type strain), the search efficiency and the ability to explore the environment can be optimized.

RESULTS

We report and compare the dynamics of three strains of *Bacillus subtilis* with different flagellar number N_f obtained by genetic manipulation (see *Materials and Methods* section for details). The strains $\Delta swrA$, wt (wild-type NCIB3610) and *swrA* have 9 ± 2 , 26 ± 6 and 41 ± 6 flagella, respectively [23] (Fig.1A). In contrast to the studies on tumbling of trapped cells [12], here we track the motion of freely swimming cells. A few typical trajectories of each strain are shown in Fig.1B, which consist of successive active run and tumble phases.

Distinct motility patterns

Strikingly, we find that the curvatures of the trajectories strongly depend on the flagellar number. The paths are clearly less curved with decreasing N_f , which may originate either from the change in their tumbling statistics or from having a larger persistence length in the run phase. While the influence of N_f on the run-and-tumble statistics will be discussed in the next section, here we focus on the latter possibility, i.e. the variations of the persistency in the run phase with changing N_f . To characterize the running persistency, we note that each run trajectory comprises a set of recorded positions of the bacterium. Given these data, one can extract the local direction of motion α and, thus, the directional change θ along the trajectory, resulting in the distribution of directional changes $P(\theta)$ [24]. Then, the persistency p of the run phase can be obtained as the Fourier transform of $P(\theta)$, i.e. $p = \int_{-\pi}^{\pi} d\theta e^{i\theta} P(\theta) = \langle \cos \theta \rangle$ [25, 26]. Alternatively, the curvature of the trajectories can be characterized by calculating the rotational mean square displacement $\text{RMSD}(\tau) = \langle (\alpha(t+\tau) - \alpha(t))^2 \rangle = 2 D_r \tau$, from which one can extract the asymptotic rotational-diffusion coef-

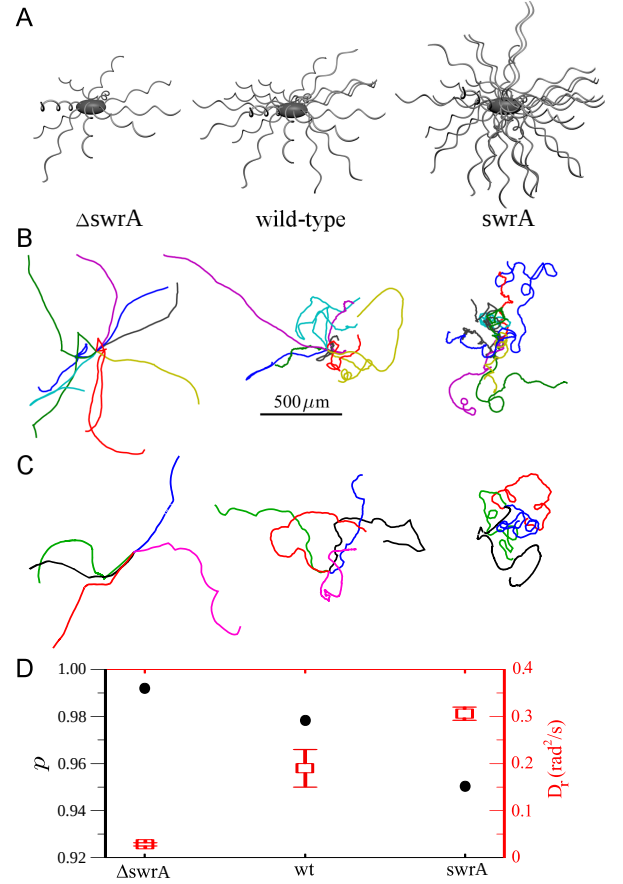


FIG. 1. **Bacterial motility patterns.** (A) Illustration of three strains of *Bacillus subtilis* with different number of flagella. (B),(C) Planar projections of quasi two-dimensional experimental (B) and simulation (C) paths. A few trajectories are randomly chosen and translated so that the first point is located at the origin. The simulation parameter values are extracted from experimental data. (D) Directional persistency of the run phase p (circles), and asymptotic rotational-diffusion coefficient D_r (squares) for different strains.

ficient D_r . The results shown in Fig.1D reveal that the directional persistency in the run phase remarkably depends on the flagellar number; the run paths are less curved for smaller N_f .

Run-and-tumble statistics

Next, we turn to studying the statistics of run and tumble events. A detailed description of the tumbling detection procedure can be found in *Materials and Methods* section. According to the results shown in Fig.2A, the tumbling speed is smaller (but non-negligible) compared to the running speed [27]. Moreover, the speeds in both run and tumble phases show no systematic dependence on N_f . A closer look at the probability distributions of the instantaneous speeds (see e.g. the running speed data in Fig.2B) reveals that even the distributions of a given strain slightly differ from one culture to another due to biological heterogeneity. Thus, there is no significant dif-

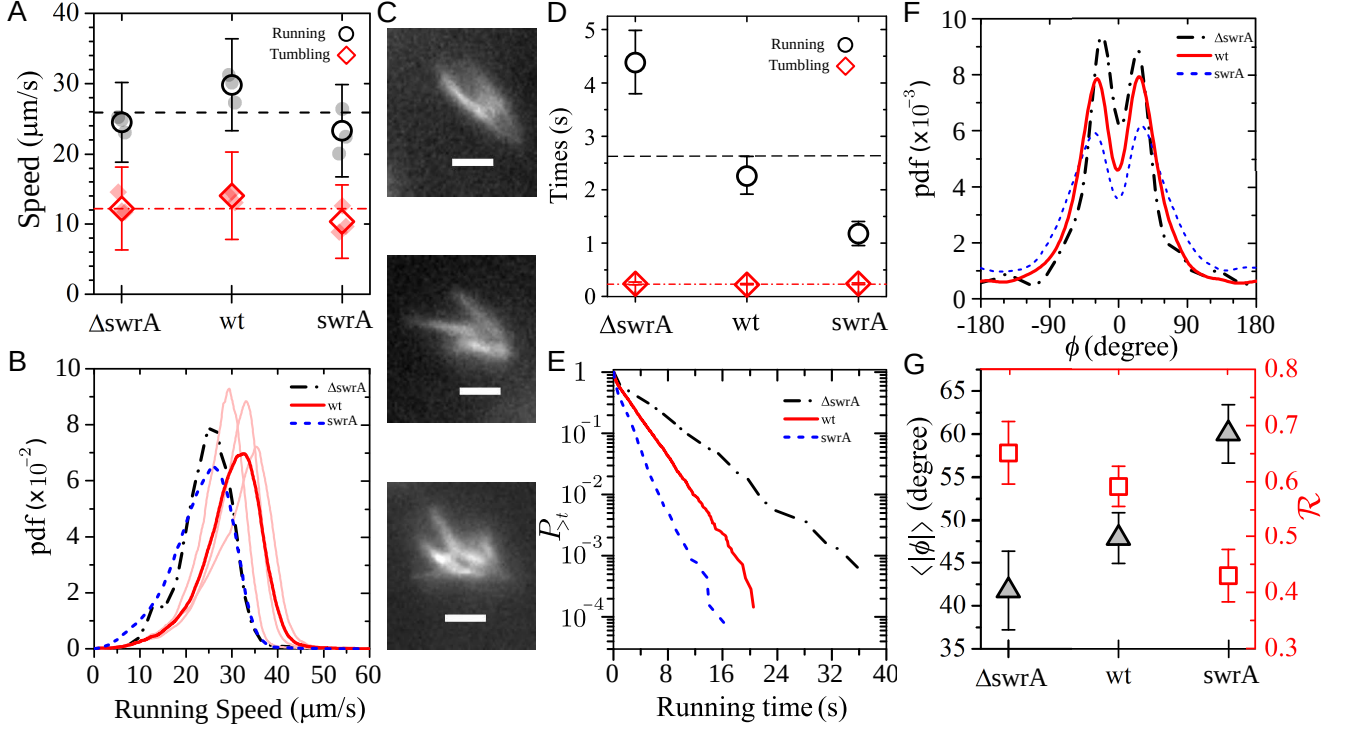


FIG. 2. **Run-and-tumble statistics.** (A) The mean run and tumble speeds for different strains (open symbols). The full symbols indicate the results for different cultures of each strain. The horizontal lines show the mean values over all strains. (B) The probability distribution of the run speed. The thin solid curves (bright red) indicate the distributions for different cultures of wt strain. (C) Fluorescence images of the bundles of a wild-type strain. Scale bar, 3.5 μm . (D) The average duration of run (circles) and tumble (diamonds) periods. The horizontal lines indicate the average values over all strains. (E) The probability distribution of observing a running time longer than a given duration t . (F) The turning-angle probability distribution $R(\phi)$. (G) The average turning angle $\langle|\phi|\rangle$ (triangles) and $\mathcal{R}=\langle\cos\phi\rangle$ (squares) for different strains.

ference in the speeds of different strains. By approximating the bundle as a single helix [4, 20, 28], simple models based on resistive-force theory predict a weak (logarithmic) growth of running speed with N_f , though experiments have shown that hydrodynamic dissipation along the cell body considerably weakens the effect [11]. Additionally, the assumption of a single bundle does not hold in general, according to our observations of fluorescently-stained flagella of swimming bacteria as well as other reports in the literature [29, 30]; even multiple bundles may form during the active running phase (several examples of a wt strain with multiple bundles are shown in Fig. 2C). The diversity of the locations and interactions between the bundles makes the prediction of the propulsive force and swimming speed highly complex.

To understand whether and to what extent the flagellar number influences the switching frequencies between run and tumble phases, we plot the average excursion times in Fig. 2D. It turns out that the mean tumbling time (~ 0.2 s) and thus the ability of restoring the run phase are not influenced by N_f . Given the mean tumbling time and speed, one finds that the displacement in the tumbling phase is of the order of the cell length (i.e. a few micrometers). However, such a swimmer with the running speed of ~ 30 $\mu\text{m/s}$ in an aqueous medium is expected to stop

after only ~ 0.6 μs and traveling approximately $0.1 A^\circ$ if the pushing force suddenly stops [31]. This suggests that the bundles are not fully disrupted in the tumbling phase, thus, the bacterium is partially propelled. The mean running times remarkably depend on the flagellar number. Increasing N_f enhances the probability of switching from running to tumbling. This supports the *veto* model for bundle disruption [13, 19], which proposes that clockwise rotation of a single or a few flagella (less than $\frac{N_f}{2}$) is sufficient to disrupt the bundle. Figure 2E shows that the tail of the probability distribution of running times is nearly exponential, with a N_f -dependent slope (data censoring for the first and last incomplete periods sharpens the trend even more). We observe similar exponential decays for the tumbling time distributions (not shown), verifying that the switching events between the two states of motility happen spontaneously and can be described by Markovian processes.

Another characteristic of the run-and-tumble dynamics that is affected by the number of flagella is the turning angle between successive run phases. We define the turning angle ϕ between two successive runs as the change in the direction of motion from the end of one run to the beginning of the next run (the direction of motion was obtained by a linear fit to four data points for each

run phase). The turning-angle distribution $R(\phi)$ obeys left-right symmetry and develops a peak for all strains. However, the peak and, more clearly, the mean of $R(\phi)$ shift towards larger angles with increasing N_f , as can be seen in Figs. 2F and 2G. Similar to the curvature of run trajectories, we can use the Fourier transform of $R(\phi)$, i.e. $\mathcal{R} = \int_{-\pi}^{\pi} d\phi e^{i\phi} R(\phi) = \langle \cos \phi \rangle$, as a measure of the directional change between consecutive run phases. \mathcal{R} ranges between -1 and 1 , with 1 , 0 , and -1 denoting 0° , 90° , and 180° turning, respectively. Indeed, \mathcal{R} is correlated with the tumbling time and speed [32] as well as the strength of the torque exerted on the cell body during the re-formation of the bundle [11]. Since the speed and excursion time in the tumbling phase are not considerably affected by N_f , we attribute the reduction of \mathcal{R} with increasing N_f to experiencing a larger torque during bundle re-formation at higher flagellar numbers [11].

We also checked that the direction of motion does not vary significantly when switching from running to tumbling. This fact and the relatively high speed in the tumbling phase once again indicate that the bundles are not fully disrupted in the tumbling phase. As a result, one expects that the tumbling is not a purely random motion and should exhibit directional persistency. To verify this idea we assign a dimensionless number $\tilde{\ell}_{\text{tumble}}$ to each tumbling segment of the trajectory, obtained by dividing the end-to-end distance by the total length of the trajectory segment. The probability distribution $P(\tilde{\ell}_{\text{tumble}})$ shown in Fig. 3A develops a sharp peak at $\tilde{\ell}_{\text{tumble}} \sim 0.9$, indicating that most of the tumbling trajectories are nearly straight during the relatively short periods of tumbling.

Finally, we measure the mean square displacement $\text{MSD}(\tau) = \langle (r(t+\tau) - r(t))^2 \rangle$ for different strains. According to our findings, the strains with lower flagellar number have less-curved run trajectories, switch less frequently from run to tumble phase, and experience a smaller turning angle between successive run phases. Consequently, the crossover from a persistent motion to the asymptotic diffusive dynamics is expected to occur at longer times for smaller values of N_f , which is confirmed by the experimental results shown in Fig. 3B. The asymptotic diffusion coefficient D is also a decreasing function of N_f (see Fig. 3C). These results indicate that for increasing the efficiency of long-distance transport, it is more beneficial to have less flagella. The strains with more flagella spend a larger fraction of time in tumbling state and have a shorter persistence length when swimming. We note that the trends (as a function of N_f) discussed in this section are robust against variations of tumbling detection thresholds.

Model

Based on our findings, we develop a stochastic coarse-grained model for a random walk with spontaneous switchings between two states of motility. We first validate the approach by comparing the analytical predictions with experimental results. Then the model enables us to better understand the influence of the flagellar num-

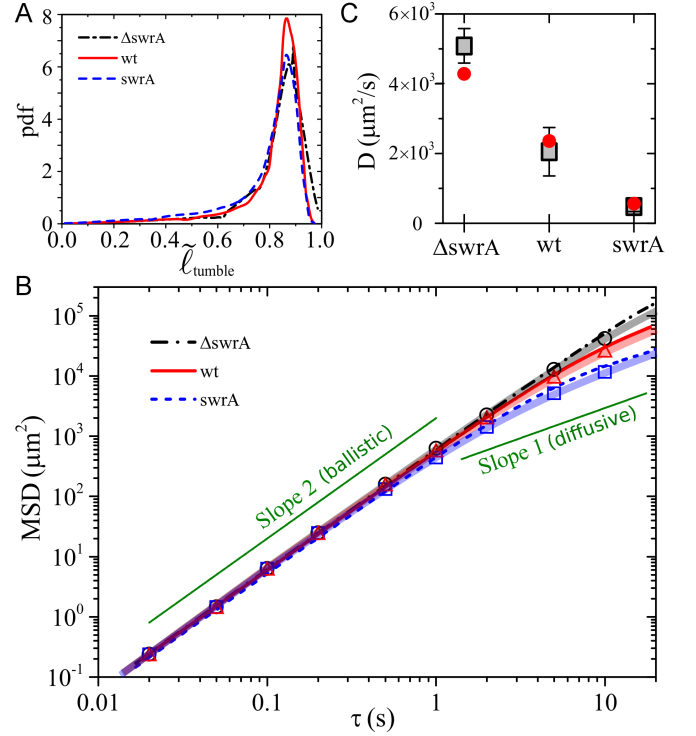


FIG. 3. **Spreading and transport properties.** (A) Probability distribution of the dimensionless quantity $\tilde{\ell}_{\text{tumble}}$, reflecting the bending of tumbling trajectories. (B) Evolution of the mean square displacement for different strains, obtained from experiments (thin dark-color lines), simulations (symbols), and the model via Eq. 13 (thick bright-color lines). (C) The asymptotic diffusion coefficient D for different strains. The analytical predictions (circles) are compared to the experimental results (squares).

ber on bacterial motility, by numerically exploring the phase space of the run-and-tumble statistical parameters and identifying the isolated role of each influential factor. Moreover, our simulations based on the two-state model evidence for a nonmonotonic dependence of the mean first-passage time on N_f .

Stochastic two-state models have been widely employed to describe altering phases of motion of e.g. swimmers and cytoskeletal motor proteins, or the locomotive patterns in other systems [33–39]. Aiming at obtaining analytical insight by including only the most prominent characteristics of the bacterial motility pattern into the model, we introduce a random walk approach in which the walker experiences two states of motility: (i) running with the mean speed v_R and persistency p , and (ii) tumbling with the mean speed v_T . The switching probabilities from run to tumble state and vice versa are supposed to be asymmetric and denoted by $f_{R \rightarrow T}$ and $f_{T \rightarrow R}$, respectively. Assuming constant switching probabilities results in exponential distributions for the residence times in each state, which is in agreement with our experimental observations. In the run state, a persistent random walk in the continuous space is considered which is char-

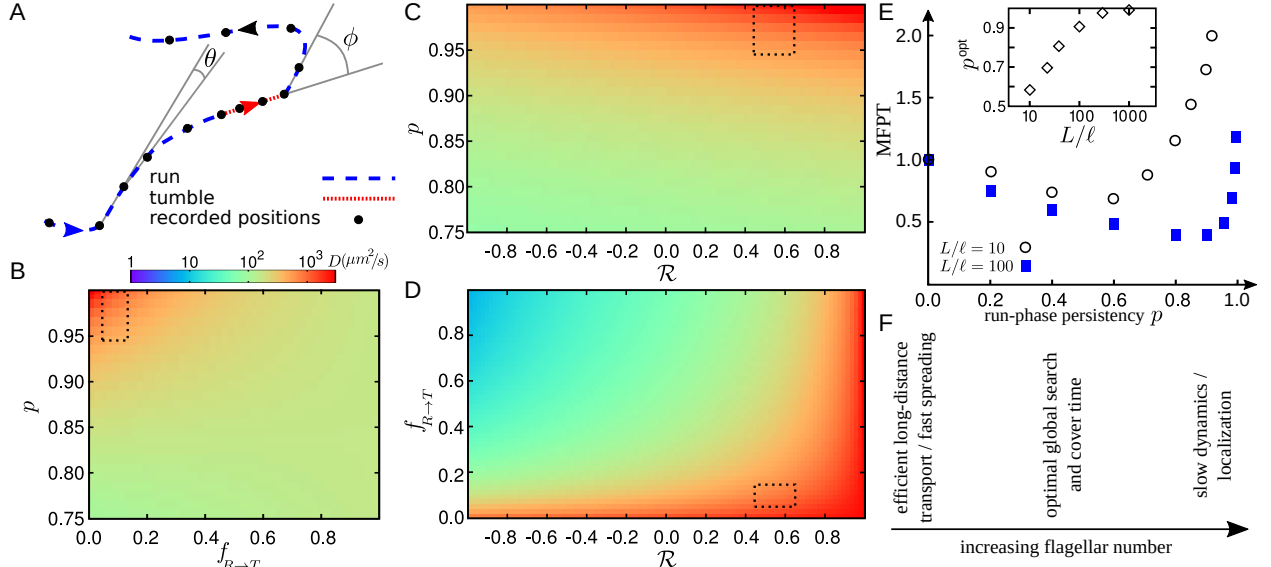


FIG. 4. **Phase diagram of the influential parameters.** (A) A typical sample trajectory of *Bacillus subtilis* with run-and-tumble dynamics. (B)-(D) Three cross-sections corresponding to (B) $\mathcal{R}=\langle\cos\phi\rangle=0.56$, (C) $f_{R\rightarrow T}=0.05$, and (D) $p=\langle\cos\theta\rangle=0.97$ of the three dimensional phase diagram in the $(\mathcal{R}, p, f_{R\rightarrow T})$ space. The color intensity reflects the magnitude of the asymptotic diffusion coefficient D . The marked regions indicate the accessible range of parameters in our experiments with *Bacillus subtilis*. (E) Mean first-passage time MFPT, scaled by MFPT at $p=0$ versus the directional persistency p of the run phase. (inset) Optimal persistency p^{opt} vs the effective system size L/ℓ . (F) Schematic picture depicting how different aspects of transport efficiency vary with N_f .

acterized by its speed v_R and the distribution $P(\theta)$ of directional changes along the run trajectory. Thus, the directional persistence $p=\int_{-\pi}^{\pi} d\theta e^{i\theta}P(\theta)=\langle\cos\theta\rangle$ quantifies the curvature of the run trajectories. Based on the results shown in Fig. 3A, the tumbling trajectories are approximated by straight lines along the last direction of motion in the run phase (see Fig. 4A). The last key property is the turning angle ϕ between two successive run phases. Using the turning-angle distribution $R(\phi)$, we calculate $\mathcal{R}=\int_{-\pi}^{\pi} d\phi e^{i\phi}R(\phi)=\langle\cos\phi\rangle$ to quantify the directional change between consecutive run phases. Denoting the time spacing between consecutive frames by Δt , we describe the process in discrete time by introducing the probability densities $P_t^R(x, y|\gamma)$ and $P_t^T(x, y|\gamma)$ to find the walker at position (x, y) along the direction γ at time t in the run and tumble states, respectively. The dynamical evolution is defined by the following set of master equations

$$\begin{aligned}
 P_{t+\Delta t}^R(x, y|\gamma) = & \\
 (1-f_{R\rightarrow T}) & \int_{-\pi}^{\pi} d\beta P(\gamma-\beta) P_t^R(x-v_R\Delta t\cos\gamma, y-v_R\Delta t\sin\gamma|\beta) \\
 + f_{T\rightarrow R} & \int_{-\pi}^{\pi} d\beta R(\gamma-\beta) P_t^T(x-v_R\Delta t\cos\gamma, y-v_R\Delta t\sin\gamma|\beta), \\
 P_{t+\Delta t}^T(x, y|\gamma) = & \\
 (1-f_{T\rightarrow R}) & P_t^T(x-v_T\Delta t\cos\gamma, y-v_T\Delta t\sin\gamma|\gamma) \\
 + f_{R\rightarrow T} & P_t^R(x-v_T\Delta t\cos\gamma, y-v_T\Delta t\sin\gamma|\gamma).
 \end{aligned} \tag{1}$$

By the two terms on the right-hand side of each equation, we consider the possibilities of being at each of the two states in the previous step. On the right-hand side of the second equation, the possibilities of moving along a straight line or switching from running to tumbling are considered. For simplicity we assume that the direction of motion does not change when switching from run to tumble state. By means of a Fourier-z-transform technique [40, 41], we obtain exact analytical expressions for temporal evolution of arbitrary moments of displacement (see *Materials and Methods* section for the details of the method and the explicit lengthy expression of MSD).

The parameter values extracted from experiments are given in Table 1 (for the calculation of p we chose $\Delta t=\frac{1}{6}$ s). Using these data as the input of the model, the time evolution of the mean square displacement can be predicted via Eq. 13 (plotted in Fig. 3B for different strains). We also performed extensive Monte Carlo simulations of a stochastic process with the same parameter values. The results agree perfectly with the analytical predictions. The agreement with experiments is also strikingly good; Despite all the simplifications, the model recovers the MSDs of all strains over the whole

Table 1: Parameter values extracted from experiments.

strain	$v_R(\frac{\mu\text{m}}{\text{s}})$	$v_T(\frac{\mu\text{m}}{\text{s}})$	$\langle t_R \rangle(\text{s})$	$\langle t_T \rangle(\text{s})$	p	\mathcal{R}
ΔswrA	24.5	12.1	4.39	0.244	0.99	0.65
wt	29.8	14.0	2.27	0.224	0.98	0.59
swrA	23.3	10.3	1.18	0.240	0.95	0.43

range of time. By introducing $A \equiv 2 \frac{f_{R \rightarrow T}}{f_{T \rightarrow R}} v_T^2 - f_{T \rightarrow R} v_R^2$ and $B \equiv 2 f_{R \rightarrow T}^2 \mathcal{R} v_T^2 + 2 f_{T \rightarrow R}^2 v_R^2$, we obtain the following expression for the asymptotic diffusion coefficient

$$D = \frac{1}{4} \frac{\Delta t}{f_{T \rightarrow R} + f_{R \rightarrow T}} \left[A + \frac{B + 2 f_{T \rightarrow R} f_{R \rightarrow T} (1 + \mathcal{R}) v_R v_T}{f_{T \rightarrow R} [1 - p - f_{R \rightarrow T} (\mathcal{R} - p)]} \right]. \quad (2)$$

The measured diffusion coefficients for different strains are in satisfactory agreement with the analytical predictions, as shown in Fig. 3C. Equation (2) reduces to the asymptotic diffusion coefficient of a single-state persistent random walker for $f_{R \rightarrow T} = 0$ and $f_{T \rightarrow R} = 1$ [42].

While it is extremely difficult to systematically vary the flagellar number in experiments, we can numerically explore the full phase space of the influential parameters. Among the key elements in determining the transport properties of the *Bacillus subtilis*, the speeds v_R and v_T , and the switching probability $f_{T \rightarrow R}$ do not vary significantly with N_f . Thus, we fix them at their average experimental values, which allows us to reduce the degrees of freedom to three sensitive parameters, i.e. \mathcal{R} , the directional persistency p , and the switching probability $f_{R \rightarrow T}$. Figures 4B-4D show 2D profiles of D in the $(\mathcal{R}, p, f_{R \rightarrow T})$ phase space, revealing that D varies by several orders of magnitude by varying these key parameters. However, limiting the parameter values to the accessible range in experiments with *Bacillus subtilis* reveals that here D and the long-distance transport are mainly affected by the variation of the run-phase persistency p . For example, by fixing the two other degrees of freedom at their average experimental values and calculating the variations of the asymptotic diffusion coefficient when the third parameter varies within the accessible range in our experiments, we get $\frac{D_{\max}}{D_{\min}} = 1.2, 1.8$, and 3.6 for varying \mathcal{R} , $f_{R \rightarrow T}$, and p , respectively. More generally, by changing the flagellar number of other types of bacteria one may deal with other regions of the 6-fold phase space.

Our analytical approach allows us to extract further information about the transport properties, such as the crossover time t_c to asymptotic diffusive regime as a function of the key parameters. The crossover time can be estimated by balancing the linear terms in time and the nonlinear contribution in the MSD equation. We find that t_c also varies by several orders of magnitude in the $(\mathcal{R}, p, f_{R \rightarrow T})$ phase space (not shown). Note that due to the interplay between the key parameters, multiple transitions between different types of anomalous diffusive dynamics occur on varying time scales in general [35].

Finally, we study the mean first-passage time (MFPT) of a two-state persistent random walk in confinement by means of extensive Monte Carlo simulations. The MFPT is defined as the mean time taken by the random walker to reach a particular position in the system for the first time. For simplicity, random walk on a cubic lattice with periodic boundary conditions is considered, and all run-and-tumble parameters except p (i.e. the most sensitive factor upon varying N_f) are

fixed at their mean experimental values. The walker is supposed to search for hidden targets during its both states of motility. The results reveal that the MFPT is a nonmonotonic function of p and admits a minimum (Fig. 4E). From the monotonic dependence of p on N_f (Fig. 1D), one concludes that the search efficiency is optimized at intermediate values of N_f . Denoting the size of the confinement with L , and the reaction range of the searcher with ℓ , the efficient persistency grows with increasing L/ℓ (inset of Fig. 4E); thus, the optimal number of flagella N_f^{opt} shifts towards smaller values with increasing the effective system size.

DISCUSSION

Our investigation of the dynamics of *Bacillus subtilis* revealed that the strains with lower flagellar number N_f have higher persistency and longer excursion time in the run phase and, additionally, their abrupt directional change when switching back to the run phase is smaller; Consequently, having too few flagella enhances the efficiency of long-distance transport (reflected e.g. in their higher translational diffusion coefficient), and causes fast spreading. Increasing the number of flagella considerably increases the probability of switching from running to tumbling as well as the curvature of the trajectories in the run phase; Moreover, switching from tumbling to running is accompanied by a larger directional change when the bacterium has more flagella. As a result, the overall orientation changes more frequently if there are too many flagella. This leads to slow dynamics and can be beneficial for the processes which require localization, such as the formation of biofilms.

However, the flagellar number of the wild-type *Bacillus subtilis* falls in the middle of the range, where the search efficiency could be optimized according to our simulation results (see Fig. 4F). Intermittent random walks are known to be beneficial for search efficiency in confined geometries [43–45]. For example, when slow diffusion periods are interrupted by fast relocating ballistic flights, it has been shown that there exists an optimal ratio between the excursion times in the two states which leads to a global minimum of the search time [43]. The optimal choice varies with the system size and the reaction range of the searcher. In addition, it has been recently shown for a single-state persistent random walk, that the mean first-passage time to find a target admits a minimum as a function of the persistency [46]. In a general two-state random walk with tumbling and persistent running phases (such as the motion of *Bacillus subtilis*), one expects that further complexity to determine the optimal search time arises due to the interplay between the directional persistency p of the run phase, the switching probabilities $f_{R \rightarrow T}$ and $f_{T \rightarrow R}$ between run and tumble (which determine the ratio between the excursion times in the two states), the size of the confinement, and the characteristics of the bacterial chemotaxis system (esp. the reaction range). However, from our experimental findings we expect

that changing the flagellar number of *Bacillus subtilis* influences the dynamics and, thus, the search time mainly via affecting the run-phase persistency p . If the number of flagella of wild-type *Bacillus subtilis* has been solely evolved towards optimizing the search efficiency, then our simulation results suggest that it should be most appropriate to live in environments with a typical size of the order of a few hundreds larger than the reaction radius of the bacterium (e.g. an environment size of less than a millimeter for a reaction radius comparable to the typical size of *Bacillus subtilis* i.e. a few microns). Our results thus provide a new insight into the nature of bacterial motility, which goes beyond the mechanochemical description of chemotaxis and mechanisms of flagellar bundle formation and disruption.

MATERIALS AND METHODS

Genetic manipulation of bacteria

Allelic replacement was performed using the pMAD-system according to [43]. All strains originated from the recently described NCIB3610 *Bacillus subtilis* strain harbouring a point mutation in the *comI* gene [44]. Briefly, the *hag* gene encoding flagellin was amplified including up- and downstream flanking regions and cloned into the pMAD plasmid. The T209 to C mutation was obtained by quick-change mutagenesis. NCIB3610 *comI*_{Q121} was transformed and positive clones selected according to [43]. Exchange of the native *hag* gene to the *hag*_{T209C} was confirmed by sequencing and light microscopy. The strain is referred to as wild-type NCIB3610 in terms of the flagellar number in the text. We are grateful to Daniel Kearns for strain DK1693 (Δ swrA, *amyE*::P_{hyspank}-swrA; *lacA*::P_{hag}-*hag*_{T209C} mls). This strain was used as both Δ swrA and swrA⁺⁺ when induced with IPTG.

Sample preparation

The temperature was set to 37°C for all steps of the experiment. First, 20 ml of frozen stock *Bacillus subtilis* was streaked onto a LB-agar plate. The plate was incubated for ~16 hours and then a few colonies of bacteria from the plate were stirred in LB and grown over night. The cultures were diluted to $OD_{600} \sim 0.1$ next morning and grown for two more hours to reach the early exponential phase within the optical density range of ~0.5 and 0.8. After dilution, swrA strain was induced by 1 mM IPTG solution to synthesize more flagella. The optical density of the cells in the exponential phase was first adjusted to 0.5 and then further diluted (~15 folds) in a fresh LB that had been previously purified by 0.4 μ m syringe filter. Because of strong sticking of Δ swrA strain to the surface, 0.005% PVP-40 (polyvinylpyrrolidones) was added before the experiments [45]. For fluorescent labeling of cells, the dye was prepared by solving 1 mg Alexa Fluor®568 C5-maleimide in 200 μ l DMSO (Dimethyl sulfoxide). 1 ml of the cell culture in $OD_{600} \sim 1$ was centrifuged at 8000g for one minute and gently washed three times in PBS pH 7.4(1X). The pellet was resuspended in

200 μ l PBS together with 5 μ l of the dye solution. The suspension was mixed and incubated in the dark at room temperature for 20 min and washed three times again in PBS buffer and re-energized by half hour outgrowth in LB to observe motile cells.

Fluorescence microscopy samples were prepared by adding 30 μ l of labeled cell suspension into a FluoroDish FD35-100 and covering it by circular cover glass (VWR, diameter 22 mm, thickness NO. 1.5). A Nikon Eclipse Ti microscope together with a Nikon N Plan Apo λ 60x, N.A. 1.4 oil immersion objective were used for fluorescence microscopy. The dye was excited by a mercury lamp and images were acquired using Hamamatsu ORCA-Flash 4.0 camera with 25 ms exposure time and 2 \times 2 binning. Tracking chamber was a superposition of a cover slip (VWR, 20 \times 20 mm, thickness NO. 1) on a microscope slide (Carl Roth GmbH, Karlsruhe, 76 \times 26 mm) separated by a thin layer of silicone grease (GE Bayer Silicones Baysilone, medium viscosity) as spacer. The chambers were quasi-two-dimensional with a height ranging between 30 and 50 μ m. The lateral sides were sealed by silicone grease after filling the cavity with bacterial suspension. Microscopy was performed with a Nikon Eclipse TE2000-s microscope and a Nikon 4x, N.A. 0.2 objective in the dark field mode. For each sample, sequences of images for 2 min with 60 Hz frame rate were recorded using a Point Grey FL3-U3-88s2cc camera. The experiments were repeated with three different cultures for each strain.

Trajectory selection and tumbling detection

A triangular smoothing filter was applied to smooth the data. Circular trajectories in the vicinity of the surface, extremely short tracks, and abnormal ones belonging to the cells in late exponential or dividing phase were discarded. More than 2500 cell trajectories were eventually selected for further analysis.

The tumbling detection algorithm was based on identifying the dramatic changes in speed $v(t)$ and magnitude of angular velocity $\omega(t)$ of the bacterium [33, 50]. First, all local minima (maxima) of v (ω) over time were deter-

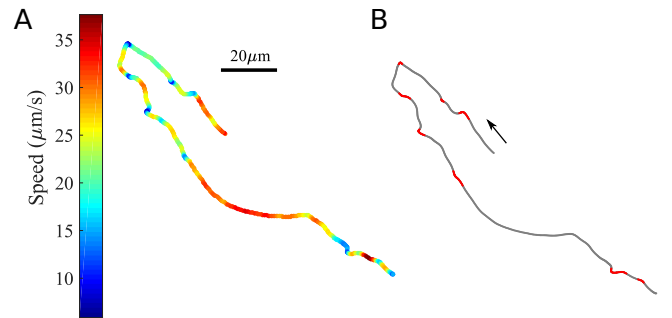


FIG. 5. **Sample trajectory with detected tumbling events.** (A) The trajectory is color coded with respect to speed. (B) The detected tumbling events are indicated with red color. The arrow shows the direction of swimming.

mined. Each minimum (maximum) is surrounded by two maxima (minima) located at t_1 and t_2 . The depth Δv of the minimum or the height $\Delta\omega$ of the maximum can be characterized as $\Delta v = \max[v(t_1) - v(t_{\min}), v(t_2) - v(t_{\min})]$ or $\Delta\omega = \max[\omega(t_{\max}) - \omega(t_1), \omega(t_{\max}) - \omega(t_2)]$, respectively. To identify a tumbling event two criteria were imposed: (i) If $\Delta v/v(t_{\min}) \geq 0.7$, there can be a tumbling phase around t_{\min} . The possible tumbling period is limited to those times t around t_{\min} where $v(t) - v(t_{\min}) \leq 0.2 \Delta v$. (ii) The local maximum of ω may indicate a tumbling event if the total directional change during the time interval $t_2 - t_1$ exceeds $\sqrt{0.8(t_2 - t_1)}$. The corresponding tumbling period consists of those times t around t_{\max} where $\omega(t_{\max}) - \omega(t) \leq \Delta\omega$. Imposing both conditions to identify a tumbling event ensures that the reduction of speed is accompanied by a sudden change in the direction of motion. See [33, 50] for more details. A sample trajectory with detected tumbling events is shown in Fig. 5 (see also *Suppl. Movie S1*).

Analytical approach

To describe the persistent motion of bacteria interrupted by stochastic tumbling periods, we developed an analytical framework for a random walker with two states of motility, as described by the set of master Eqs. 1. In the following, we briefly explain how arbitrary moments of displacement can be obtained by a Fourier-z-transform technique. Here, a two-dimensional motion is considered but extension to three dimensions is straightforward. The Fourier transform of $P_t^j(x, y|\gamma)$ is defined as

$$P_t^j(\omega|m) \equiv \int_{-\pi}^{\pi} d\gamma e^{im\gamma} \int dy \int dx e^{i\omega \cdot r} P_t^j(x, y|\gamma), \quad (3)$$

with $j \in \{R, T\}$. An arbitrary moment of displacement $\langle x^{k_1} y^{k_2} \rangle^j(t)$ can be obtained as

$$\begin{aligned} \langle x^{k_1} y^{k_2} \rangle^j(t) &\equiv \int d\gamma \int dy \int dx x^{k_1} y^{k_2} P_t^j(x, y|\gamma) \\ &= (-i)^{k_1+k_2} \frac{\partial^{k_1+k_2} P_t^j(\omega_x, \omega_y|m=0)}{\partial \omega_x^{k_1} \partial \omega_y^{k_2}} \Big|_{(\omega_x, \omega_y)=(0,0)}. \end{aligned} \quad (4)$$

The master Eqs. 1 after Fourier transformation read

$$\begin{aligned} P_{t+\Delta t}^R(\omega, \alpha|m) &= \sum_{k=-\infty}^{\infty} i^k e^{-ik\alpha} J_k(\omega v_R \Delta t) \left[f_{T \rightarrow R} \mathcal{R}(m+k) P_t^T(\omega, \alpha|m+k) \right. \\ &\quad \left. + (1 - f_{R \rightarrow T}) p(m+k) P_t^R(\omega, \alpha|m+k) \right], \end{aligned} \quad (6)$$

$$\begin{aligned} P_{t+\Delta t}^T(\omega, \alpha|m) &= \sum_{k=-\infty}^{\infty} i^k e^{-ik\alpha} J_k(\omega v_T \Delta t) \left[f_{R \rightarrow T} P_t^R(\omega, \alpha|m+k) \right. \\ &\quad \left. + (1 - f_{T \rightarrow R}) P_t^T(\omega, \alpha|m+k) \right], \end{aligned} \quad (7)$$

where we used the k th order Bessel's function

$$J_k(z) = \frac{1}{2\pi i^k} \int_{-\pi}^{\pi} d\gamma e^{iz \cos \gamma} e^{-ik\gamma}, \quad (8)$$

the Fourier transforms of the turning-angle distribution

$$\mathcal{R}(m) = \int_{-\pi}^{\pi} d\phi e^{im\phi} R(\phi), \quad (9)$$

and the distribution of the directional change along the run trajectory

$$p(m) = \int_{-\pi}^{\pi} d\theta e^{im\theta} R(\theta). \quad (10)$$

The Fourier transform of the probability $P_t^j(\omega, \alpha|m)$ can be expanded as a Taylor series

$$\begin{aligned} P_t^j(\omega, \alpha|m) &= Q_{0,t}^j(\alpha|m) + i\omega v_j \Delta t Q_{1,t}^j(\alpha|m) \\ &\quad - \frac{1}{2} \omega^2 v_j^2 (\Delta t)^2 Q_{2,t}^j(\alpha|m) + \dots, \end{aligned} \quad (11)$$

and the moments of displacement can be read in terms of the Taylor expansion coefficients. For example,

$$\langle x^2 \rangle^j(t) = v_j^2 (\Delta t)^2 Q_{2,t}^j(0|0). \quad (12)$$

Thus we expand both sides of the master equations 6 and 7 and collect all terms with the same power in ω . As a result, coupled recursion relations for the Taylor expansion coefficients of terms with the same power in ω can be obtained. Next, the time indices on both sides of these equations can be equalized by means of z -transform, which enables us to obtain the moments of displacement in the z -space. For example, one obtains the following exact expression for the mean square displacement

$$\begin{aligned} \langle x^2 \rangle(z) &= \sum_{t=0}^{\infty} z^{-t} \langle x^2 \rangle(t) = \\ &= (\Delta t)^2 \left[v_R^2 Q_2^R(z, 0|0) + v_T^2 Q_2^T(z, 0|0) \right] = \\ &= (\Delta t)^2 \left[(1 - f_{R \rightarrow T}) Q_0^R(z, 0|0) + f_{T \rightarrow R} Q_0^T(z, 0|0) \right] \times \\ &\quad \left[\frac{z \left[z - (1 - f_{T \rightarrow R}) \right]}{(z-1)G(z)} v_R^2 + \frac{z}{(z-1)G(z)} f_{R \rightarrow T} v_R v_T - \frac{1}{2(z-1)} v_R^2 \right] \\ &\quad + (\Delta t)^2 \left[f_{R \rightarrow T} Q_0^R(z, 0|0) + (1 - f_{T \rightarrow R}) Q_0^T(z, 0|0) \right] \times \\ &\quad \left[\frac{z \left[z - (1 - f_{T \rightarrow R}) p \right]}{(z-1)G(z)} v_T^2 + \frac{z}{(z-1)G(z)} f_{T \rightarrow R} \mathcal{R} v_R v_T - \frac{1}{2(z-1)} v_T^2 \right], \end{aligned} \quad (13)$$

where

$$G(z) = \left[z - (1 - f_{T \rightarrow R}) \right] \left[z - (1 - f_{R \rightarrow T}) p \right] - f_{R \rightarrow T} f_{T \rightarrow R} \mathcal{R}. \quad (14)$$

By inverse z -transforming the moments of displacement in the z -space, the moments can be obtained as a function of time.

SUPPLEMENTARY MATERIALS

movie S1. A sample bacterial trajectory.

-
- [1] H. C. Berg, *E. coli in motion* (Springer Verlag, New York), (2004).
 - [2] J. Schuhmacher, K. M. Thormann, G. Bange, How bacteria maintain location and number of flagella. *FEMS Rev. Microbiol.* **39**, 812-822 (2015).
 - [3] H. C. Berg, R. A. Anderson, Bacteria swim by rotating their flagellar filaments. *Nature* **245**, 380-382 (1973).
 - [4] E. Lauga, T. R. Powers, The hydrodynamics of swimming microorganisms. *Rep. Prog. Phys.* **72**, 096601 (2009).
 - [5] H. C. Berg, D. A. Brown, Chemotaxis in escherichia coli analysed by three-dimensional tracking. *Nature* **239**, 500-504 (1972).
 - [6] O. Benichou, M. Coppey, M. Moreau, P. H. Suet, R. Voituriez, Optimal search strategies for hidden targets. *Phys. Rev. Lett.* **94**, 198101 (2005).
 - [7] F. Bartumeus, S. A. Levin, Fractal reorientation clocks: Linking animal behavior to statistical patterns of search. *Proc. Natl. Acad. Sci.* **105**, 19072 (2008).
 - [8] O. Benichou, C. Loverdo, M. Moreau, R. Voituriez, Intermittent search strategies. *Rev. Mod. Phys.* **83**, 81-129 (2011).
 - [9] G. H. Wadhams, J. P. Armitage, Making sense of it all: bacterial chemotaxis. *Nat. Rev. Mol. Cell Biol.* **5**, 1024-1037 (2004).
 - [10] S. Chattopahyay, R. Moldovan, C. Yeung, X. L. Wu, Swimming efficiency of bacterium escherichia coli. *Proc. Natl. Acad. Sci.* **103**, 13712-13717 (2006).
 - [11] N. C. Darnton, L. Turner, S. Rojevsky, H. C. Berg, On torque and tumbling in swimming escherichia coli. *J. Bacteriol.* **89**, 1756-1764 (2007).
 - [12] P. J. Mears, K. Santosh, C. V. Rao, I. Golding, Y. R. Chemla, Escherichia coli swimming is robust against variations in flagellar number. *Elife* **3**, e01916 (2014).
 - [13] L. Turner, W. S. Ryu, H. C. Berg, Real-time imaging of fluorescent flagellar filaments. *J. Bacteriol.* **182**, 2793-2801 (2000).
 - [14] E. A. Korobkova, T. Emonet, H. Park, P. Cluzel, Hidden stochastic nature of a single bacterial motor. *Phys. Rev. Lett.* **96**, 058105 (2006).
 - [15] S. Terasawa, H. Fukuoka, Y. Inoue, T. Sagawa, H. Takahashi, A. Ishijima, Coordinated reversal of flagellar motors on a single escherichia coli cell. *Biophys. J.* **100**, 2193-2200 (2011).
 - [16] B. Hu, Y. Tu, Coordinated switching of bacterial flagellar motors: evidence for direct motor-motor coupling? *Phys. Rev. Lett.* **110**, 158703 (2013).
 - [17] J. Hu, M. Yang, G. Gompfer, R. G. Winkler, Modelling the mechanics and hydrodynamics of swimming E. coli. *Soft Matter* **11**, 7867-7876 (2015).
 - [18] N. Vladimirov, D. Lebedez, V. Sourjik, Predicted auxiliary navigation mechanism of peritrichously flagellated chemotactic bacteria. *PLoS Comput. Biol.* **6**, e1000717 (2010).
 - [19] N. W. Sneddon, W. Pontius, T. Emonet, Stochastic coordination of multiple actuators reduces latency and improves chemotactic response in bacteria. *Proc. Natl. Acad. Sci.* **109**, 805-810 (2012).
 - [20] P. Kanehl, T. Ishikawa, Fluid mechanics of swimming bacteria with multiple flagella. *Phys. Rev. E* **89**, 042704 (2014).
 - [21] S. Y. Reigh, R. G. Winkler, G. Gompfer, Synchronization and bundling of anchored bacterial flagella. *Soft Matter* **8**, 4363-4372 (2012).
 - [22] D. B. Kearns, R. Losick, Cell population heterogeneity during growth of *Bacillus subtilis*. *Genes Dev.* **19**, 3083-3094 (2005).
 - [23] S. B. Guttenplan, S. Shaw, D. B. Kearns, The cell biology of peritrichous flagella in *Bacillus subtilis*. *Mol. Microbiol.* **87**, 211-229 (2013).
 - [24] S. Burov *et al.*, Distribution of directional change as a signature of complex dynamics. *Proc. Natl. Acad. Sci.* **110**, 19689-19694 (2013).
 - [25] M. R. Shaebani, Z. Sadjadi, I. M. Sokolov, H. Rieger, L. Santen, Anomalous diffusion of self-propelled particles in directed random environments. *Phys. Rev. E* **90**, 030701(R) (2014).
 - [26] Z. Sadjadi, M. R. Shaebani, H. Rieger, L. Santen, Persistent random walk approach to anomalous transport of self-propelled particles. *Phys. Rev. E* **91**, 062715 (2015).
 - [27] L. Turner, L. Ping, M. Neubauer, H. C. Berg, Visualizing flagella while tracking bacteria. *Biophys. J.* **111**, 630-639 (2016).
 - [28] B. Rodenborn, C.-H. Chen, H. L. Swinney, B. Liu, H. P. Zhang, Propulsion of microorganisms by a helical flagellum. *Proc. Natl. Acad. Sci.* **110**, E338-E347 (2013).
 - [29] C. Valeriani, M. Li, J. Novosel, J. Arlt, D. Marenduzzo, Colloids in a bacterial bath: simulations and experiments. *Soft Matter* **7**, 5228-5238 (2011).
 - [30] Y. Hyon, T. R. Powers, R. Stocker, H. C. Fu, The wiggling trajectories of bacteria. *J. Fluid Mech.* **705**, 58-76 (2012).
 - [31] E. M. Purcell, Life at low Reynolds number. *Am. J. Phys.* **45**, 3-11 (1977).
 - [32] J. Saragosti, P. Silberzan, A. Buguin, Modeling E. coli tumbles by rotational diffusion: Implications for chemotaxis. *PLoS ONE* **7**, e35412 (2012).
 - [33] M. Theves, J. Taktikos, V. Zaburdaev, H. Stark, C. Beta, A bacterial swimmer with two alternating speeds of propagation. *Biophys. J.* **105**, 1915-1924 (2013).
 - [34] J. Taktikos, H. Stark, V. Zaburdaev, How the motility pattern of bacteria affects their dispersal and chemotaxis. *PLoS ONE* **8**, e81936 (2013).
 - [35] A. E. Hafner, L. Santen, H. Rieger, M. R. Shaebani, Run-and-pause dynamics of cytoskeletal motor proteins. *Sci. Rep.* **6**, 37162 (2016).
 - [36] I. Pinkoviezky, N. S. Gov, Transport dynamics of molecular motors that switch between an active and inactive state. *Phys. Rev. E* **88**, 022714 (2013).
 - [37] M. R. Shaebani, A. E. Hafner, L. Santen, Geometrical considerations for anomalous transport in complex neuronal dendrites. *submitted* (2017).
 - [38] M. Kong, Y. Wu, G. Liab, R. G. Larson, A bead-spring model for running and tumbling of flagellated swimmers: detailed predictions compared to experimental data for E. coli. *Soft Matter* **11**, 1572-1581 (2015).
 - [39] N. Watari, R. G. Larson, The hydrodynamics of a run-and-tumble bacterium propelled by polymorphic helical flagella. *Biophys. J.* **98**, 12-17 (2010).
 - [40] Z. Sadjadi, M. F. Miri, M. R. Shaebani, S. Nakhaee, Diffusive transport of light in a two-dimensional disordered packing of disks: Analytical approach to transport mean free path. *Phys. Rev. E* **78**, 031121 (2008).
 - [41] Z. Sadjadi, M. F. Miri, Diffusive transport of light in two-dimensional granular materials. *Phys. Rev. E* **84**, 051305 (2011).
 - [42] P. Tierno, M. R. Shaebani, Enhanced diffusion and anomalous transport of magnetic colloids driven above a two-state flashing potential. *Soft Matter* **12**, 3398-3405 (2016).
 - [43] O. Benichou, C. Loverdo, M. Moreau, R. Voituriez, Two-dimensional intermittent search processes: An alternative to Levy flight strategies. *Phys. Rev. E* **74**, 020102 (2006).
 - [44] M. Chabaud *et al.*, Cell migration and antigen capture are antagonistic processes coupled by myosin II in dendritic cells.

- Nat. Commun.* **6**, 7526 (2015).
- [45] J. F. Rupprecht, O. Benichou, R. Voituriez, Optimal search strategies of run-and-tumble walks. *Phys. Rev. E* **94**, 012117 (2016).
 - [46] V. Tejedor, R. Voituriez, O. Benichou, Optimizing persistent random searches. *Phys. Rev. Lett.* **108**, 088103 (2012).
 - [47] M. Arnaud, A. Chastanet, M. Débarbouillé, New vector for efficient allelic replacement in naturally nontransformable, low-GC-content, gram-positive bacteria. *Appl. Environ. Microbiol.* **70**, 6887-6891 (2004).
 - [48] M. A. Konkol, K. M. Blair, D. B. Kearns, Plasmid-Encoded ComI Inhibits Competence in the Ancestral 3610 Strain of *Bacillus subtilis*. *J. Bacteriol.* **195**, 4085-4093 (2013).
 - [49] A. P. Berke, L. Turner, H. C. Berg, E. Lauga, Hydrodynamic attraction of swimming microorganisms by surfaces. *Phys. Rev. Lett.* **101**, 038102 (2008).
 - [50] J. B. Masson, G. Voisinnea, J. Wong-Nga, A. Celania, M. Vergassolaa, Noninvasive inference of the molecular chemotactic

response using bacterial trajectories. *Proc. Natl. Acad. Sci.* **109**, 1802-1807 (2012).

Acknowledgments: We thank Daniel B. Kearns for providing us with strain DK1693, and Z. Sadjadi for fruitful discussions. **Funding:** M. R. S. acknowledges support by DFG within SFB 1027 (A7). **Author contributions:** C. W. and G. B. designed the research. F. A. prepared the strains of the bacterium *Bacillus subtilis*. C. W., T. J., and J. N. designed and built the experimental setup. J. N. carried out the experiments and analyzed the results. M. R. S. developed the analytical model and performed simulations. All authors contributed to the interpretation of the results. M. R. S. drafted the manuscript. **Competing interests:** The authors declare that they have no competing interests. **Data and materials availability:** All data needed to evaluate the conclusions in the paper are present in the paper. Additional data related to this paper may be requested from the authors.